Philosophical Magazine
Vol. 89, Nos. 34–36, 1–21 December 2009, 3351–3369

Taylor & Francis
Taylor & Francis Group

Atomistic simulations of cross-slip nucleation at screw dislocation intersections in face-centered cubic nickel

S.I. Rao[a], D.M. Dimiduk[b], J.A. El-Awady[c], T.A. Parthasarathy[a], M.D. Uchic[b] and C. Woodward[b]*

[a]*UES, Inc., 4401 Dayton-Xenia Rd, Dayton, OH 45432-1894, USA;* [b]*Air Force Research Laboratory, Materials and Manufacturing Directorate, AFRL/MLLM Wright-Patterson AFB, OH 45433-7817, USA;* [c]*UTC, Dayton, OH 45432, USA*

(*Received 16 June 2009; final version received 25 August 2009*)

The Escaig model for thermally activated cross-slip in face-centered cubic (fcc) materials assumes that cross-slip preferentially occurs at obstacles that produce large stress gradients on the Shockley partials of the screw dislocations. However, it is unclear as to the source, identity and concentration of such obstacles in single-phase fcc materials. Embedded atom potential, molecular-statics simulations of screw character dislocation intersections with 120° forest dislocations in fcc Ni are described that illustrate a mechanism for cross-slip nucleation. The simulations show how such intersections readily produce cross-slip nuclei and thus may be preferential sites for cross-slip. The energies of the dislocation intersection cores are estimated and it is shown that a partially cross-slipped configuration for the intersection is the most stable. In addition, simple three-dimensional dislocation dynamics simulations accounting for Shockley partials are shown to qualitatively reproduce the atomistically determined core structures for the same dislocation intersections.

Keywords: cross-slip; dislocation intersections; atomistic simulations; embedded atom potentials; dislocation dynamics simulations

1. Introduction

There is an increasing recognition of the need to incorporate physics-based models of deformation in design of structural components. Whereas models for predicting yield strength and creep behavior are beginning to incorporate significant physics, models for fatigue and ultimate strength remain mostly empirical. This is because strain-hardening and fatigue resistance are highly influenced by dislocation micromechanisms, e.g. cross-slip, and including physics-based cross-slip processes in mesoscale simulations (e.g. dislocation dynamics) has been difficult. The early work of Escaig remains the most widely cited and used model for cross-slip (see Figure 1) [1–4]; however, this model poses several difficulties with respect to quantitative simulations. The model is highly sensitive to choice of parameters that

*Corresponding author. Email: christopher.woodward@wpafb.af.mil

ISSN 1478–6435 print/ISSN 1478–6443 online

DOI: 10.1080/14786430903286201
http://www.informaworld.com

Report Documentation Page

Form Approved
OMB No. 0704-0188

1. REPORT DATE	2. REPORT TYPE	3. DATES COVERED
DEC 2009		**00-00-2009 to 00-00-2009**

4. TITLE AND SUBTITLE	5a. CONTRACT NUMBER
Atomistic Simulations of Cross-slip Nucleation at Screw Dislocation Intersections in Face-centered Cubic Nickel	5b. GRANT NUMBER
	5c. PROGRAM ELEMENT NUMBER
6. AUTHOR(S)	5d. PROJECT NUMBER
	5e. TASK NUMBER
	5f. WORK UNIT NUMBER
7. PERFORMING ORGANIZATION NAME(S) AND ADDRESS(ES) **UES Inc,4401 Dayton-Xenia Rd,Dayton,OH,45432-1894**	8. PERFORMING ORGANIZATION REPORT NUMBER
9. SPONSORING/MONITORING AGENCY NAME(S) AND ADDRESS(ES)	10. SPONSOR/MONITOR'S ACRONYM(S)
	11. SPONSOR/MONITOR'S REPORT NUMBER(S)

12. DISTRIBUTION/AVAILABILITY STATEMENT
Approved for public release; distribution unlimited

13. SUPPLEMENTARY NOTES

14. ABSTRACT

15. SUBJECT TERMS

16. SECURITY CLASSIFICATION OF:			17. LIMITATION OF ABSTRACT	18. NUMBER OF PAGES	19a. NAME OF RESPONSIBLE PERSON
a. REPORT	b. ABSTRACT	c. THIS PAGE			
unclassified	**unclassified**	**unclassified**	**Same as Report (SAR)**	**19**	

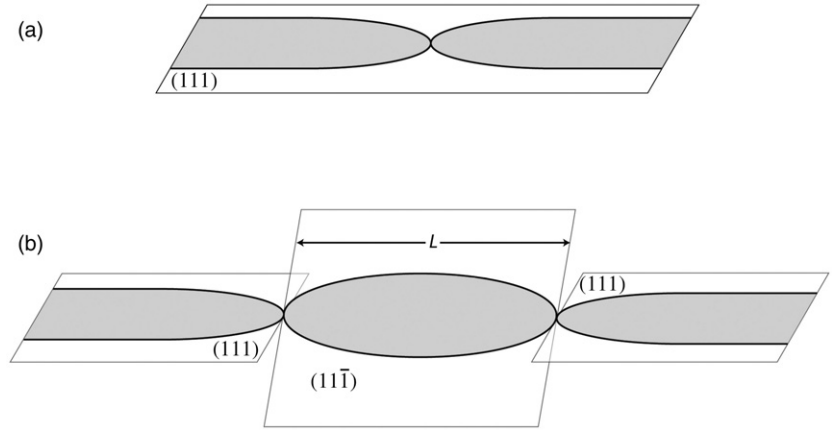

Figure 1. Illustration of the activation energy for cross-slip in Escaig's model: separation of a Stroh constriction into a negative and a positive constriction.

have thus far been difficult to obtain. For example, the constriction width required for cross-slip is unknown but significantly influences the energetics of the cross-slip process [5]. This difficulty has led to an *ad hoc* postulate that obstacles always exist in materials and that they enable sufficient dislocation core constriction under stresses, thereby ensuring cross-slip [1]. Aside from being unsatisfactory, this forces cross-slip models (particularly for single crystals) to make arbitrary assumptions about dislocation obstacle spacings. Advances in atomistic simulations make it possible to gain insights into the cross-slip process and may serve to inform mesoscale simulations to accurately capture the atomic-level physics of that dislocation process.

Atomistic simulation works to date have been limited to calculating constriction energies and energetics of cross-slip using a single dislocation in a periodic unit cell [6,7]. These simulations helped to unravel some interesting and potentially useful aspects of cross-slip. The most important finding was that there exists configurations where one of the pair of constrictions has a negative energy (negative constriction) and the other has a large positive energy (positive constriction) [6,7]. Thus, spontaneous nucleation of cross-slip is possible so long as only one constriction is needed, as is the case for surface cross-slip nucleation [8]. These previous simulations found that the total energy of a pair of constrictions, required for cross-slip within the bulk of a solid, from a pre-existing constriction (Stroh constriction, see Figure 1) is always positive. The energy of a Stroh constriction can be shown to be a mean of the energies of the negative and positive constrictions [9]. The simulations predict relatively high energies for cross-slip (>1 eV) that thermal activation would require substantial stress to activate at temperatures where cross-slip is observed experimentally. This does not address the problem of having to assume *ad hoc* obstacles that permit stress build-up in mesoscale simulations.

In the early 1960s, Washburn [10] suggested that cross-slip in fcc materials preferentially occurs at dislocation intersections with other forest dislocations residing on the cross-slip plane that form collinear locks and glide locks [10,11].

Table 1. Reactions and locks that occur between a $\frac{1}{2}[1\bar{1}0]$ screw dislocation and forest dislocations on the $(11\bar{1})$, $(1\bar{1}1)$ and $(1\bar{1}\bar{1})$ planes. The screw dislocation is considered to reside completely, either on the glide (111) or the cross-slip $(11\bar{1})$ plane.

			Lock	
Plane	Burgers vector	Reaction	Glide	Cross-slip
$11\bar{1}$	$-\frac{1}{2}[1\bar{1}0]$	$\frac{1}{2}[1\bar{1}0]-\frac{1}{2}[1\bar{1}0]=0$	Collinear	Annhilation
$11\bar{1}$	$-\frac{1}{2}[101]$	$\frac{1}{2}[1\bar{1}0]-\frac{1}{2}[101]=\frac{1}{2}[0\bar{1}\bar{1}]$	Glide	Reaction
$11\bar{1}$	$\frac{1}{2}[011]$	$\frac{1}{2}[1\bar{1}0]+\frac{1}{2}[011]=\frac{1}{2}[101]$	Glide	Reaction
$1\bar{1}1$	$-\frac{1}{2}[110]$	$\frac{1}{2}[1\bar{1}0]-\frac{1}{2}[110]=[0\bar{1}0]$	Hirth	Hirth
$1\bar{1}1$	$-\frac{1}{2}[10\bar{1}]$	$\frac{1}{2}[1\bar{1}0]-\frac{1}{2}[10\bar{1}]=\frac{1}{2}[0\bar{1}1]$	Glide	Lomer–Cottrell
$1\bar{1}1$	$\frac{1}{2}[011]$	$\frac{1}{2}[1\bar{1}0]+\frac{1}{2}[011]=\frac{1}{2}[101]$	Lomer–Cottrell	Glide
$1\bar{1}\bar{1}$	$-\frac{1}{2}[110]$	$\frac{1}{2}[1\bar{1}0]-\frac{1}{2}[110]=[0\bar{1}0]$	Hirth	Hirth
$1\bar{1}\bar{1}$	$-\frac{1}{2}[101]$	$\frac{1}{2}[1\bar{1}0]-\frac{1}{2}[101]=\frac{1}{2}[0\bar{1}\bar{1}]$	Lomer–Cottrell	Glide
$1\bar{1}\bar{1}$	$\frac{1}{2}[01\bar{1}]$	$\frac{1}{2}[1\bar{1}0]+\frac{1}{2}[01\bar{1}]=\frac{1}{2}[10\bar{1}]$	Glide	Lomer–Cottrell

However, there has been little to no investigation of those ideas since that time. In this work, we expand on the ideas of Washburn. We consider screw dislocation intersections with forest dislocations residing on the two other {111} type planes, other than forest dislocations residing on the cross-slip {111} type plane. If we take the screw dislocation as having a $\frac{1}{2}[1\bar{1}0]$ Burgers vector residing on the (111) plane with the $(11\bar{1})$ plane being the cross-slip plane, the intersections that are of importance for cross-slip are intersections with the $(1\bar{1}1)$ and $(1\bar{1}\bar{1})$ planes. Table 1 gives the locks that are formed, as well as the reaction product, for intersections with different Burgers vectors on these two planes as well as the cross-slip plane. In Table 1, the locks that are formed are written down for two cases: (i) the screw dislocation is completely residing on the glide (111) plane and (ii) the screw dislocation is completely residing on the cross-slip $(11\bar{1})$ plane. From Table 1, it is clear that, by symmetry, the intersections with the $(1\bar{1}1)$ plane are identical to the intersections with the $(1\bar{1}\bar{1})$ plane, and therefore, one needs to consider only the screw dislocation intersections with the $(1\bar{1}1)$ plane. Also, considering that the screw dislocation can completely reside on the glide (111) or the cross-slip $(11\bar{1})$ plane, the intersection with the $\frac{1}{2}[\bar{1}01]$ Burgers vector on the $(1\bar{1}1)$ plane can be shown by symmetry to be equivalent to the intersection with the $\frac{1}{2}[011]$ Burgers vector on the $(1\bar{1}1)$ plane. As a result, one needs to consider only the intersections with the $\frac{1}{2}[\bar{1}01]$ and the $\frac{1}{2}[\bar{1}\bar{1}0]$ Burgers vectors on the $(1\bar{1}1)$ plane. For the $\frac{1}{2}[\bar{1}01]$ Burgers vector, the intersection results in a Lomer–Cottrell barrier if the screw dislocation is on the cross-slip $(11\bar{1})$ plane or, a glide barrier if the screw dislocation is residing on the glide (111) plane. For the $\frac{1}{2}[\bar{1}\bar{1}0]$ Burgers vector, the intersection results in a Hirth lock irrespective of whether the screw dislocation resides on the glide plane or the cross-slip plane. The common direction (junction direction) between the screw direction glide plane, (111) and the intersecting $(1\bar{1}1)$ plane is $[\bar{1}01]$ and the common direction between the screw direction cross-slip plane, $(11\bar{1})$ and the $(1\bar{1}1)$ plane is [011]. Due to the fact that the junction direction as well as the type of lock that is formed is dependent on whether the screw dislocation resides on the glide plane

or the cross-slip plane, the energies of these intersections may be expected to depend strongly on the plane in which the screw dislocation resides. This may enhance the possibility of local cross-slip at the intersection region.

In this work, the possibility of cross-slip at dislocation–dislocation intersections was selectively examined using large-scale atomistic simulations that contain more than one dislocation. A glide dislocation that intersects a pair of forest dislocations is modeled and it is shown that several conditions exist where cross-slip can nucleate. This, we believe, has the potential of allowing simulations of cross-slip in larger scale discrete dislocation dynamics simulations and provides a better physical basis for cross-slip and perhaps to provide a realistic statistical representation of cross-slip during monotonic or cyclic deformation.

We have performed molecular statics simulations of screw-character dislocation intersections ($\frac{1}{2}[1\bar{1}0]$ Burgers vector) with both the $\frac{1}{2}[\bar{1}01]$ and the $\frac{1}{2}[\bar{1}\bar{1}0]$ Burgers vectors on the $(1\bar{1}1)$ plane. We have considered several line orientations for the intersecting dislocation over a 180° range (all orientations where the intersection is expected to be attractive). For the sake of clarity, we restrict ourselves to results only for the screw (and near-screw) dislocation intersection, with the $\frac{1}{2}[\bar{1}01]$ Burgers vector residing on the $(1\bar{1}1)$ plane with the 120° $\langle 0\bar{1}\bar{1}\rangle$ line orientation. Section 2 describes the simulation technique and the interatomic potential used for the simulations, and Section 3 presents the core structures and the energies obtained from atomistic simulations and dislocation dynamics (DD) simulations for these specific intersections. Finally, Sections 4 and 5 give a discussion and summary, respectively, of the results.

2. Simulation technique

The atomistic simulations described here employed the three-dimensional (3D) parallel molecular dynamics code, LAAMPS [12], developed at Sandia National Laboratory. A schematic of the simulation cell used in the atomistic simulations is shown in Figure 2. The simulation cell is a rectangular parallelepiped with the x-axis oriented along $[1\bar{1}0]$, y-axis along $[11\bar{2}]$ and the z-axis along [111]. The dimensions of the simulation cell are 62.0 nm along the x-axis and 31.5 nm along both the y- and z-axes corresponding to a simulation cell of 5,405,160 atoms. A $\frac{1}{2}[1\bar{1}0]$ screw-character dislocation is inserted in the middle of the simulation cell using its anisotropic elastic displacement field [13]. Similarly, two 120° dislocations, having a Burgers vector of $\frac{1}{2}[\bar{1}01]$ and line directions $\langle 0\bar{1}\bar{1}\rangle$ spaced 30.0 nm apart (at $x = -15.0$ and 15.0 nm, with y, $z \sim 0$), were also introduced into the simulation cell using their anisotropic elastic displacement fields. The origin for the initial anisotropic displacement field of the screw and 120° dislocations were varied (ten different origins were used) to obtain several different core structures for the screw dislocation intersection. For simplicity, fixed boundary conditions were applied along all three directions and energy minimization was performed using the conjugate gradient technique. A couple of simulations were performed using periodic boundary conditions along the screw or 'x' direction. In these cases, the two intersecting dislocations were opposite in character (+120° and −60°), such that periodic boundary conditions could be applied.

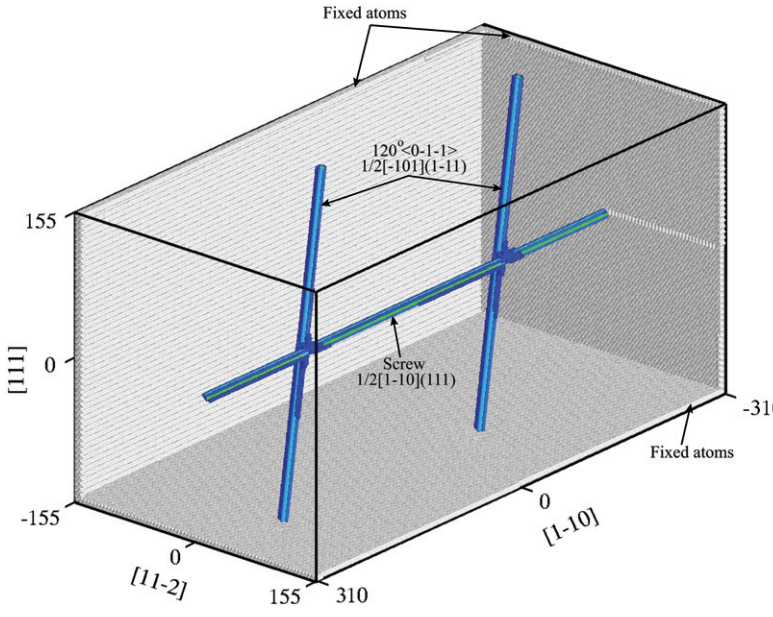

Figure 2. A schematic of the simulation cell used in the atomistic simulations described in this manuscript. The axes dimensions are in units of Å.

Table 2. Lattice parameter, a_0, cohesive energy, E_c, elastic constants C_{11}, C_{12} and C_{44}, and stacking fault energy, γ, given by the Ni Angelo–Moody–Baskes EAM potential.

Property	Value
a_0	0.352 nm
C_{11}	$2.464 \times 10^{11}\,\mathrm{N\,m^{-2}}$
C_{12}	$1.473 \times 10^{11}\,\mathrm{N\,m^{-2}}$
C_{44}	$1.248 \times 10^{11}\,\mathrm{N\,m^{-2}}$
E_c	−4.45 eV
γ	$0.089\,\mathrm{J\ m^{-2}}$

2.1. *Interatomic potential*

The embedded atom potential used in the simulations was developed for fcc Ni by Angelo et al. [14] based on the Voter and Chen format. Table 2 gives the lattice parameter, cohesive energy, elastic constants and stacking fault energy given by the potential for fcc Ni. The stacking fault energy, $\sim$90 mJ m^{-2}, lies inbetween a value of 60 and 120 mJ m^{-2}, the values given by the two Ni potentials that Rao et al. [6] used in previous atomistic simulations of bulk cross-slip.

2.2. *Depiction of core structures*

In order to illustrate the relaxed intersection geometries, we take advantage of the increase in atomic energy produced by the strain field of the partial dislocations.

By plotting the atoms with assigned energies of greater than −4.42 eV (the approximate energy of atoms in the stacking fault region) the partial dislocations can be visualized easily even in these large simulation cells. In order to illustrate the cross-slipped-segment products of the intersections, the positions are shown in a $[11\bar{2}]$ projection (i.e. the x–z plane) as well as the [111] projection (i.e the x–y plane). In the $[11\bar{2}]$ projection segments spread on the initial (111) plane appear as a single line and cross-slipped segments (i.e. on a $(1\bar{1}1)$ plane) appear as a pair of partials separated by a stacking fault. The projection along the y-axis provides a quick indicator of whether the screw dislocation is residing on the (111) glide plane or the $(1\bar{1}1)$ cross-slip plane or a combination of both.

2.3. *Dislocation dynamics simulations*

The core structures obtained for the intersection using atomistic simulations were reproduced using a simple dislocation dynamics (DD) method, DDLab, originally developed at Lawrence Livermore National Laboratory [15]. DDLab runs within MATLAB and is intended for simulations having a limited number of dislocation lines while taking into account the Shockley partials [16]. A $\frac{1}{2}[1\bar{1}0]$] screw dislocation and a 120° intersecting dislocation (line direction $\langle 0\bar{1}\bar{1}\rangle$, Burgers vector $\frac{1}{2}[\bar{1}01]$) split into their respective Shockley partials (2.0 nm apart), 70 nm in length and fixed at both ends, were initially introduced into an infinite simulation cell and allowed to relax under no applied stress. The screw character dislocation was initially taken to be either completely dissociated on the glide (111) plane, completely dissociated on the cross-slip $(11\bar{1})$ plane or, partly dissociated on the glide (111) plane and partly on the cross-slip $(11\bar{1})$ plane. The 120° dislocation was initially taken to go through the origin of the simulation box, whereas the screw dislocation was initially taken to be ±3.0 nm away from the origin along the 'y'-axis ($[11\bar{2}]$). The relaxed configurations were compared with results from atomistic simulations.

3. Atomistic core structures for the intersection

Figure 3 depicts [111] and $[11\bar{2}]$ projections (i.e. the 'x–y' and 'x–z' planes) of one of the core structures obtained for the screw dislocation −120° dislocation intersection, glide lock (Gl1) configuration. In this case, the screw dislocation was initially positioned a $[11\bar{2}]$ unit along the positive 'y'-axis (+0.8 nm), away from the origin. The original placement of the threading and cutting dislocations allows the dislocation cores to interact and combine as dictated by the geometry and Peach–Koehler forces as generated thorough the interatomic potentials. The screw dislocation fully resides on the glide (111) plane and is constricted at both the intersections (Stroh constrictions [17]) around one of the Shockley partials of the 120° $\frac{1}{2}[\bar{1}01]$ dislocation residing on the $(1\bar{1}1)$ plane. Due to the fixed boundary conditions along 'x' (which mimic a jog on the screw dislocation at the fixed boundaries), the screw dislocation is constricted in its glide plane at both ends near the boundary, which is equivalent to a full Stroh constriction [17]. Therefore, in order to obtain the estimates of the energy for the intersection core structure

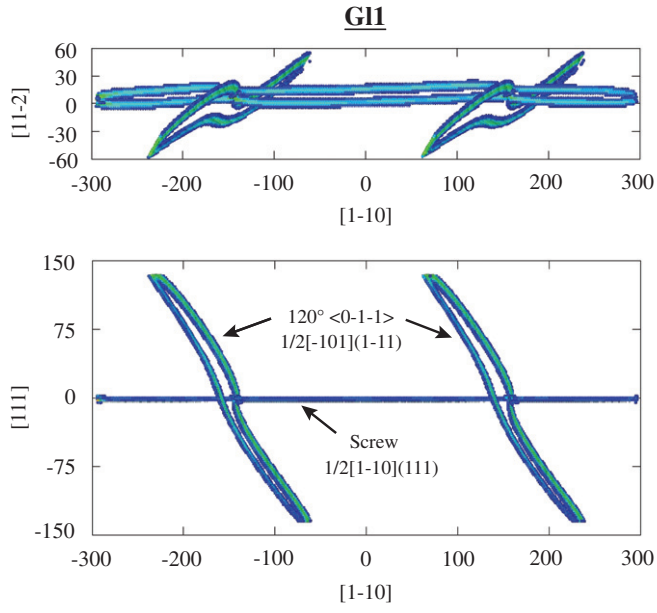

Figure 3. [111] (x–y plane) and [11$\bar{2}$] (x–z plane) projections of the core structure (Gl1) for a screw −120° intersection in fcc Ni from atomistic simulations. Atoms with energy greater than the energy at a stacking fault are plotted. The axes dimensions are in units of Å.

Gl1 without any jogs, the energy of a 'Stroh' constriction needs to be subtracted from the energy of this core structure.

Figure 4 depicts two of the core structures obtained for the screw dislocation −120° dislocation intersection, Lomer–Cottrell lock configurations (LC1 and LC2), that were obtained using a slightly different elastic center for the initial anisotropic displacement field of the screw and 120° dislocations, as compared to Figure 3. The [111] and [11$\bar{2}$] projections are shown for each case. In Figure 4a, the screw dislocation was initially positioned a [11$\bar{2}$] unit along the negative 'y'-axis (+0.8 nm), away from the origin. In Figure 4b, the screw dislocation was initially positioned a [11$\bar{2}$] unit along the positive 'y'-axis (−0.8 nm), away from the origin. After relaxation, Figures 4a and b, the screw dislocation fully resides on the cross-slip (11$\bar{1}$) plane. In Figure 4b, as in Figure 3, the screw dislocation is constricted at both the intersections around one of the Shockley partials of the 120° ½[$\bar{1}$01] dislocation residing on the (1$\bar{1}$1) plane. In Figure 4a, the a/6[$\bar{1}$12] Shockley partial of the screw dislocation combines with the a/6[1$\bar{2}\bar{1}$] Shockley partial of the 120° dislocation to form an extended node with a resulting short Burgers vector of the type 1/6[0$\bar{1}$1], or Lomer–Cottrell barrier. At the other end of the Lomer–Cottrell barrier, the screw dislocation is constricted to form one half of a Stroh constriction. Since the interaction between the 1/6[0$\bar{1}$1] Burgers vector and the other Shockley partial of the 120° dislocation (a/6[2$\bar{1}$1]) is weak, the 120° dislocation needs to constrict significantly to attain a lower separation distance at the extended node reaction region. Also, as in Figure 3, due to the fixed boundary conditions along 'x', the screw

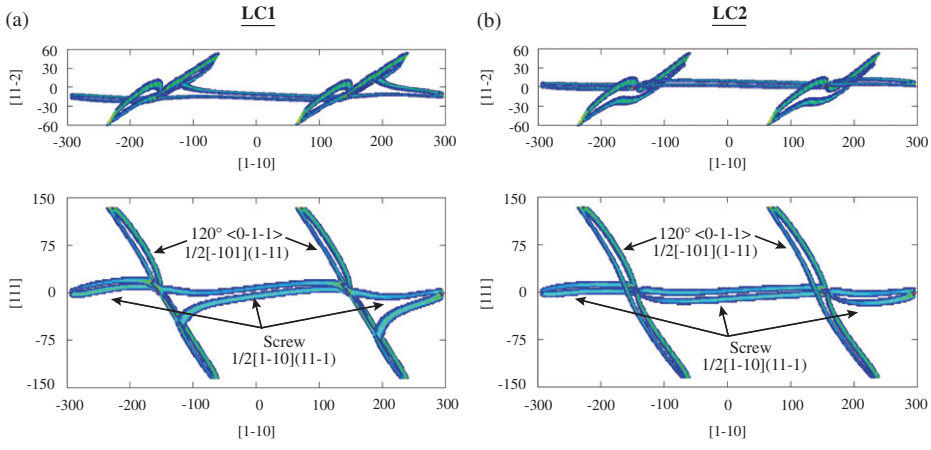

Figure 4. [111] (x–y plane) and [11$\bar{2}$] (x–z plane) projections of the core structures (LC1 and LC2) for a screw –120° intersection in fcc Ni from atomistic simulations. Atoms with energy greater than the energy at a stacking fault are plotted. The axes dimensions are in units of Å.

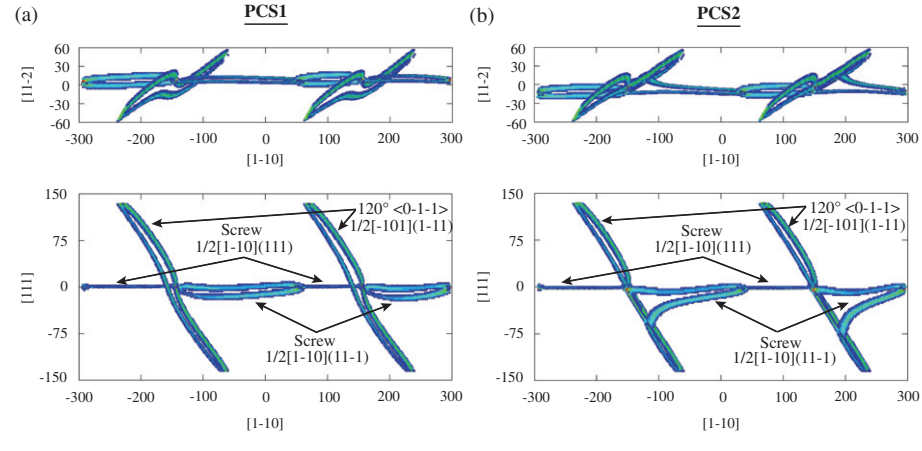

Figure 5. [111] (x–y plane) and [11$\bar{2}$] (x–z plane) projections of the core structures (PCS1 and PCS2) for a screw –120° intersection in fcc Ni from atomistic simulations. Atoms with energy greater than the energy at a stacking fault are plotted. The axes dimensions are in units of Å.

dislocation forms the equivalent of a 'Stroh' constriction at its ends and this energy has to be subtracted to obtain the true energy of intersection core structures LC1 and LC2 without any jogs.

Figure 5 depicts two of the relaxed core structures for the screw dislocation −120° dislocation intersection, partially cross-slipped locks (PCS1 and PCS2), that were obtained using a slightly different elastic center for the initial anisotropic

displacement field of the screw and 120° dislocations, as compared to Figures 3 and 4. The [111] and [11$\bar{2}$] projections are shown for each case. In Figure 5a, the screw dislocation was initially positioned a [11$\bar{2}$] unit along the positive '*y*'-axis (+0.8 nm), away from the origin. In Figure 5b, the screw dislocation was initially positioned a [11$\bar{2}$] unit along the negative '*y*'-axis (−0.8 nm), away from the origin. In both cases, after relaxation, the screw dislocation is partially on the glide (111) plane and partially on the cross-slip (11$\bar{1}$) plane. This is in essence the presence of cross-slip nuclei at these intersections. These results are similar to previous observations of athermal cross-slip nucleation at screw dislocation interactions with Frank interstitial loops in fcc Ni [18]. In Figure 5a, as in Figure 3, the screw dislocation is constricted at both the intersections (negative constrictions [6,7]) around one of the Shockley partials of the 120° ½[$\bar{1}$01] dislocation residing on the (1$\bar{1}$1) plane. Since the core is in the partially cross-slipped state, a companion positive constriction [6,7] forms between the intersections. In Figure 5b, as in Figure 4a, the a/6[$\bar{1}$12] Shockley partial of the screw dislocation combines with the a/6[1$\bar{2}$$\bar{1}$] Shockley partial of the 120° dislocation to form an extended node with a resulting short Burgers vector of the type 1/6[0$\bar{1}$1], Lomer–Cottrell barrier. At the other end of the Lomer–Cottrell barrier, the screw dislocation is constricted to form one half of a negative constriction and is cross-slipped onto the glide (111) plane. Since the core is in the partially cross-slipped state, a companion full positive constriction [6,7] forms between the intersections. As in Figure 4a, since the interaction between the 1/6[0$\bar{1}$1] Burgers vector and the other Shockley partial of the 120° dislocation is weak, the 120° dislocation needs to constrict significantly to attain a lower separation distance at the extended node reaction region. Due to the fixed boundary conditions along '*x*', the screw dislocation is constricted at both ends near the boundary in both Figures 5a and 5b, forming what is equivalent to a full positive constriction [6,7]. In this case, this behavior can be interpreted as the natural formation of a positive constriction inbetween intersections and no energy correction is required to obtain the energy of core structures PCS1 and PCS2.

3.1. *Energetics of the atomistic intersection core structures*

The energy of the cells was evaluated as a function of size in order to assess the errors introduced by the finite nature of the simulation volume and boundary conditions. This is accomplished by calculating the energy differences between core structures truncated at different finite distances along the '*y*' and '*z*' directions. Figure 6 shows a plot of the relative energy of three different core structures obtained for the screw −120° intersection as a function of the distance along '*y*' and '*z*'. The energy is calculated for cells of lengths 5.0, 7.5, 10.0 and 12.5 nm along '*y*' and '*z*' and the energy difference obtained between the different core structures is plotted as a function of these cell sizes. Curve (a) in Figure 6 is a plot of the energy differences between two identical core structures obtained for the intersection (Figure 3, fully residing on the glide (111) plane) with two different initial elastic centers and shows that the measurement of relative energy has an error of the order of 0.2 eV using this technique. The partially cross-slipped configuration (PCS1) is stable

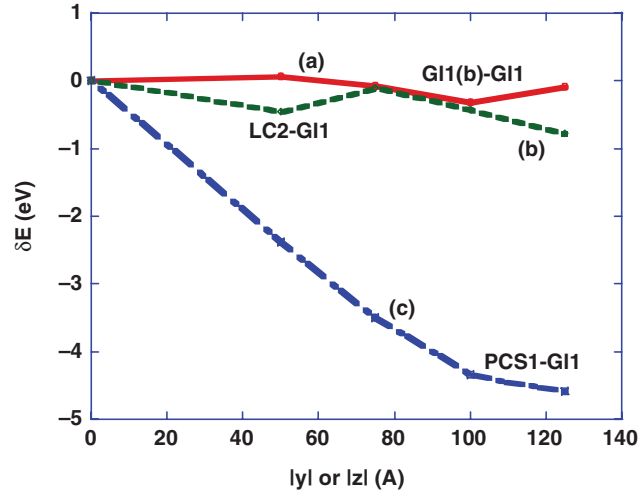

Figure 6. Relative energies of the core structures, Gl1, LC2 and PCS1, plotted as a function of the truncation distance along 'y' and 'z'. Two instantiations of the core structure Gl1 are also compared with each other to determine the accuracy in the relative energy measurement. The axes dimensions are in units of Å.

Table 3. Relative energies of various core structures obtained atomistically for the screw dislocation −120° dislocation intersection.

Core	Relative energy (eV)
GL1	0
LC1	5.3
LC2	−0.8
PCS1	−4.6
PCS2	5.8

relative to the cores Gl1 (fully residing on the glide plane) and LC2 (fully residing on the cross-slip plane) by 4–4.6 eV and the energy difference values are fairly converged at a distance of 125 Å along 'y' and 'z'. If one subtracts the bulk Stroh constriction energy (∼1.9 eV, estimated as a mean of the negative and positive constriction energies at a stacking fault energy of 90 mJ m^{-2} [6]) from the energy of the core structures Gl1 and LC2, for reasons stated in Section 3.0, one obtains that the partially cross-slipped configuration is stable relative to Gl1 and LC2 by 2.1–2.7 eV, or 1–1.3 eV per intersection. These results show that the energy of a negative constriction is significantly lowered at the intersections, relative to the bulk, due to the stress field of the intersecting dislocations. Table 3 gives the relative energy values for the five different core structures shown in Figures 3–5 obtained using the technique described above with a truncation distance along 'y' and 'z' of 12.5 nm, without the Stroh constriction correction.

These results suggest that cross-slip nuclei are readily available at these intersections and that cross-slip nucleation at these intersections is relatively easy in fcc Ni. Also, the energy of core structures with extended nodes (obtained when the screw dislocation was initially placed a [112] unit along the negative '*y*'-axis, LC1 and PCS2) is significantly larger than the core structures which have no extended nodes (obtained when the screw dislocation was initially placed a [112] unit along the positive '*y*'-axis, Gl1, LC2 and PCS1). This may be related to the constriction of the 120° dislocations that is required to form the extended node.

3.2. *Check of initial conditions to the atomistic simulations*

For the atomistic simulations described above, the initial separation between the screw and the intersecting 120° dislocations was kept at 0.85 nm, similar to what was used in previously published atomistic simulations of dislocation intersections [19]. In order to assess the effect of the initial separation distance between the intersecting dislocations, several simulations were performed with increasing initial separation distance between the intersecting dislocations, in steps of 0.85 nm, up to a separation distance of 4.3 nm. In all cases, the partially cross-slipped configuration, with the formation of cross-slip nuclei, was observed, even when the stand-off distance exceed the equilibrium spacing for the Shockley partial dislocations of a relaxed core. Figure 7 shows a plot of one of the atomistic core structures observed for the intersection when the initial separation distance between the intersecting dislocations was kept at 3.4 nm. This suggests that a small initial separation distance ($\sim$1.0 nm) between the intersecting dislocations does not significantly affect the atomistic simulation results. Investigation of further increases in the initial separation distance requires larger simulation cell sizes than used here because of the fixed boundary conditions along all three directions.

Secondly, the initial character of the screw-character dislocation was made to deviate from the perfect screw orientation in steps of 2° up to a deviation of 6°. Again, in all cases, the partially cross-slipped configuration, with the formation of cross-slip nuclei, was observed. Figure 8 shows a plot of the observation of a partially cross-slipped configuration for the intersection in atomistic simulations, when the initial nearly screw-character dislocation was oriented 4° away from the perfect screw orientation, with a direction of [52 −48 −4]. Again, further tilting of the screw-character dislocation requires larger simulation cell sizes than used here.

Finally, in all the simulations described above, two 120° intersecting dislocations having a separation distance of 30 nm were used, in order to minimize the effect of fixed boundaries along the *x*-axis. The separation distance of 30 nm corresponds approximately to a dislocation density of $10^{15}\,\mathrm{m}^{-2}$, which is representative of the upper limits of densities in heavily worked materials and is typical of what may be found in substructure walls. A simulation was run where the separation distance between the two intersecting 120° dislocations was increased by a factor of 3, to 92.5 nm, and the simulation cell size along the *x*-axis was also increased by a factor of 3, to 185 nm. This separation distance corresponds approximately to a dislocation density of $10^{14}\,\mathrm{m}^{-2}$. Figure 9 shows the partially cross-slipped configuration with the formation of cross-slip nuclei observed in atomistic simulations under these

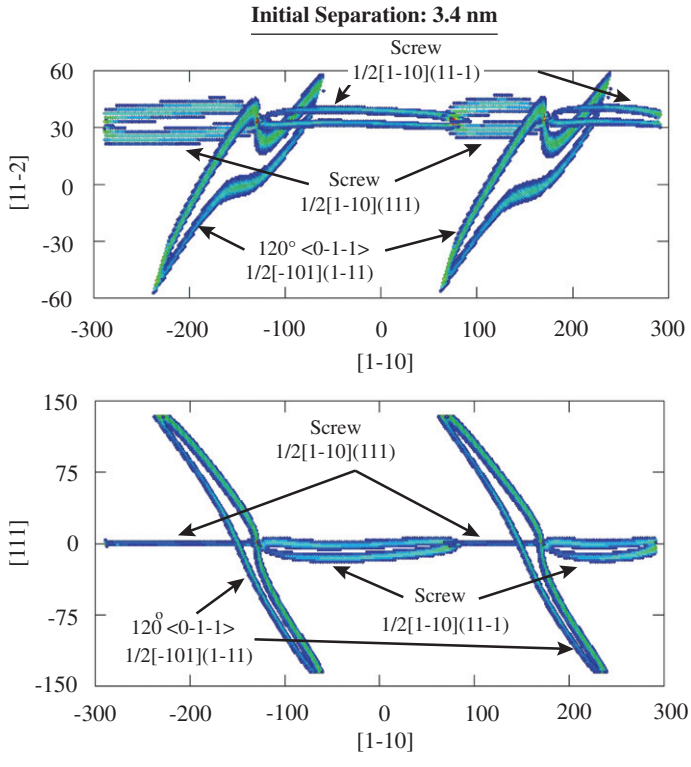

Figure 7. [111] (x–y plane) and [11$\bar{2}$] (x–z plane) projections of the partially-cross slipped core structure for a screw –120° intersection in fcc Ni from atomistic simulations when the initial separation distance between the screw and intersecting dislocations was kept at 3.4 nm. Atoms with energy greater than the energy at a stacking fault are plotted. The axes dimensions are in units of Å.

conditions. In addition, in order to check whether the presence of two intersecting 120° dislocations has a significant effect on the simulations described above, a simulation was performed with only a single intersecting dislocation, at the center of the simulation cell. Once again, the partially cross-slipped configuration, with the formation of cross-slip nuclei, was observed, as shown in Figure 10.

3.3. *Periodic boundary condition atomistic simulations*

Several simulations were performed imposing periodic boundary conditions along the screw (x or 1$\bar{1}$0) direction. Such boundary conditions could be imposed only by making the two intersecting dislocations opposite or dipole in character (+120° and −60°). Fixed boundary conditions were still imposed along the 'y' and 'z' directions. Figure 11 shows a plot of two different core structures obtained for the intersection using four different elastic centers for the initial anisotropic displacement field, with periodic boundary conditions imposed along the 'x' direction.

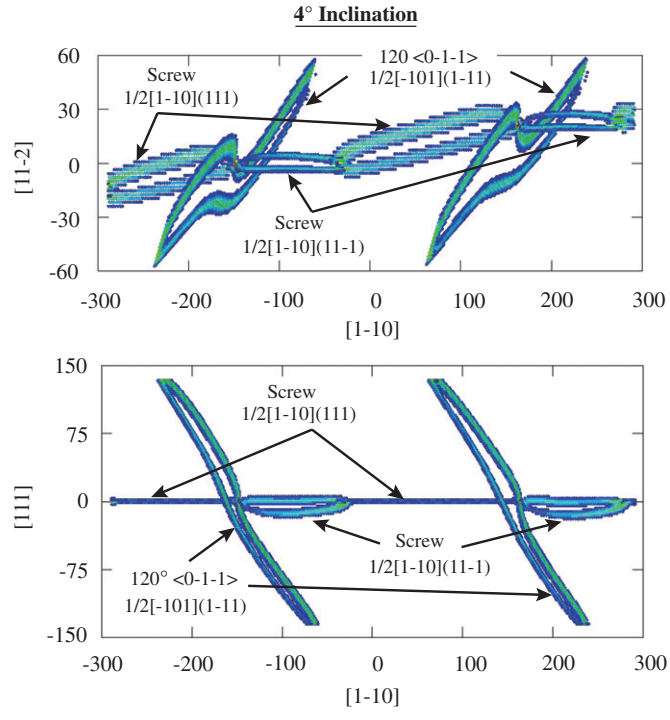

Figure 8. [111] (x–y plane) and [11$\bar{2}$] (x–z plane) projections of the partially-cross-slipped core structure for a screw –120° intersection in fcc Ni from atomistic simulations when the initial direction of the nearly screw character dislocation was [52 −48 −4]. Atoms with energy greater than the energy at a stacking fault are plotted. The axes dimensions are in units of Å.

In both cases, the screw dislocation is partially cross-slipped onto the cross-slip (11$\bar{1}$) plane. In Figure 11a, the screw dislocation is partially cross-slipped at the +120° intersection, whereas in Figure 11b, it is partially cross-slipped at both the +120° and −60° intersections. These results suggest that the partially cross-slipped configuration forms even at the repulsive −60° intersection.

3.4. *Dislocation dynamics simulations*

Figure 12 shows a plot of the structure of a 120° intersection core obtained using 3D dislocation dynamics simulations. The dislocation dynamics simulation results are compared with the corresponding core structure obtained for the 120° intersection with atomistic simulations. Here, the screw dislocation was initially placed in the 3D dislocation dynamics simulation cell as partially cross-slipped onto the cross-slip (11$\bar{1}$) plane. The node transitioning the screw dislocation from the (111) glide plane to the cross-slip (11$\bar{1}$) plane was free to move along the screw [1$\bar{1}$0] direction. Figure 12 shows that the partially cross-slipped configuration for the 120° intersection core is stable and good correspondence is found between the dislocation

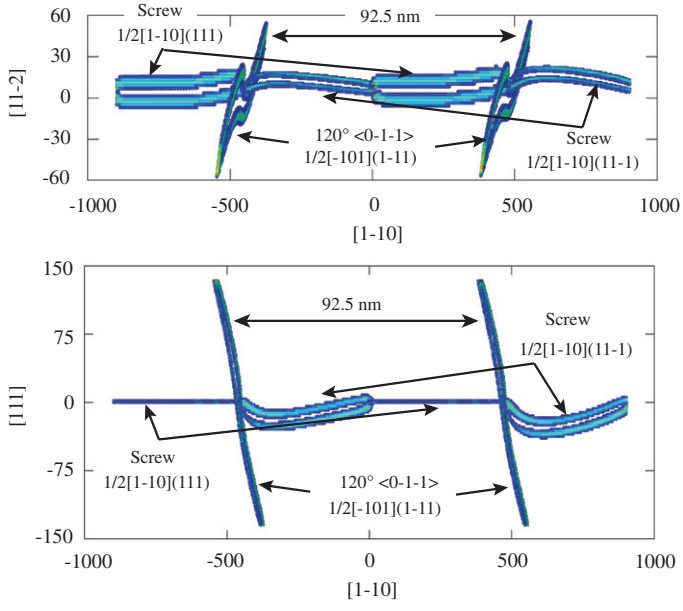

Figure 9. [111] (x–y plane) and [11$\bar{2}$] (x–z plane) projections of the partially-cross-slipped core structure for a screw $-120°$ intersection in fcc Ni from atomistic simulations when only a single intersecting dislocation at the center of the simulation cell was used. Atoms with energy greater than their energy at a stacking fault are plotted. The axes dimensions are in units of Å.

dynamics and atomistic simulation results. We conclude that the elastic interactions of the partial dislocations and the ensuing recombination of the partials at the junctions capture the essential details of the dislocation evolution within the atomistic simulations. Similar dislocation dynamics simulations were found to reproduce all the five core structures (Figures 3–5) predicted by the atomistic simulations.

4. Discussion

The results of this work clearly show that several dislocation configurations exist within fcc crystals containing forest dislocations, where a glide dislocation can nucleate a cross-slip event. The atomistic simulation results show that cross-slip nuclei are readily available at near-screw dislocation intersections with forest dislocations residing on the two {111} planes other than the cross-slip plane forming one of Lomer–Cottrell, glide or Hirth locks.

This mechanism of cross-slip nucleation is in addition to other mechanisms of obstacle induced cross-slip initiation, like cross-slip at screw dipoles, jogs, surfaces, etc. [8,20,21]. However, the probability of dislocation intersections is relatively large as compared to other mechanisms of obstacle induced cross-slip. Also, cross-slip at screw dipoles, jogs and surfaces is athermal only under specific

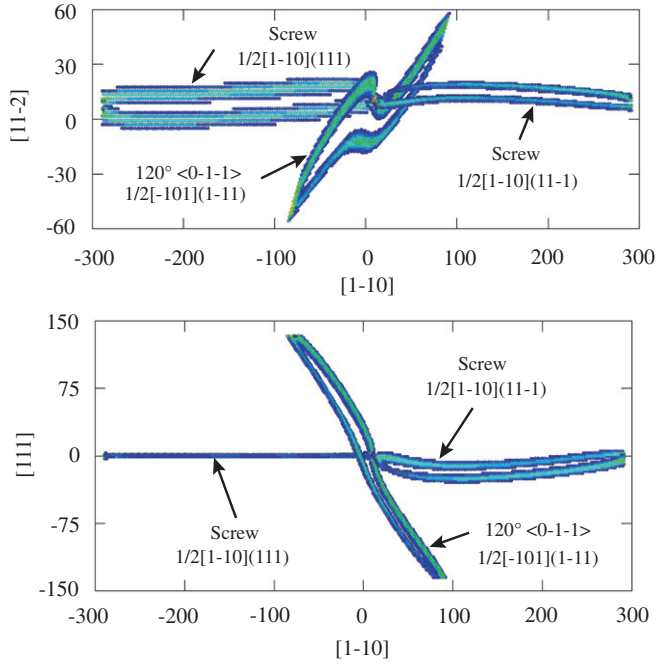

Figure 10. [111] (x–y plane) and [11$\bar{2}$] (x–z plane) projections of the partially-cross-slipped core structure for a screw −120° intersection in fcc Ni from atomistic simulations where the separation between the two intersecting 120° dislocations was 92.5 nm. Atoms with energy greater than the energy at a stacking fault are plotted. The axes dimensions are in units of Å.

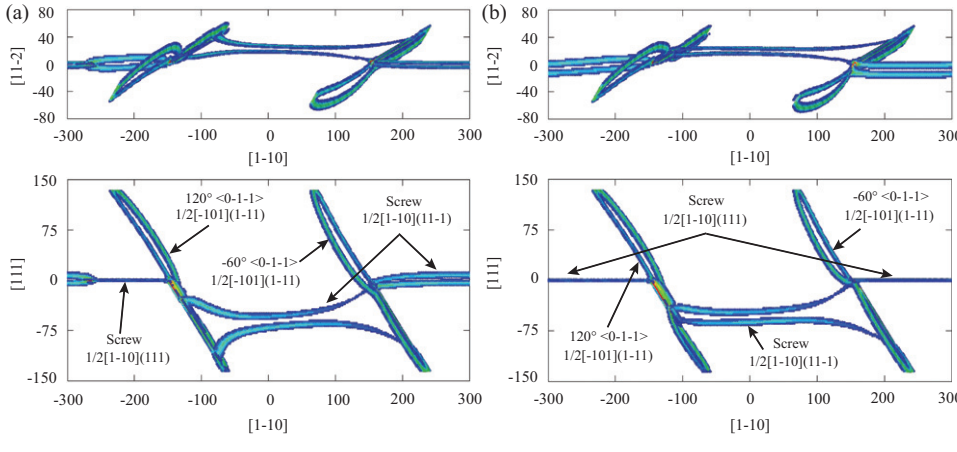

Figure 11. [111] (x–y plane) and [11$\bar{2}$] (x–z plane) projections of two different core structures obtained for screw −120° and −60° intersections in fcc Ni from atomistic simulations with periodic boundary conditions along the screw or 'x' direction. Atoms with energy greater than the energy at a stacking fault are plotted. The axes dimensions are in units of Å.

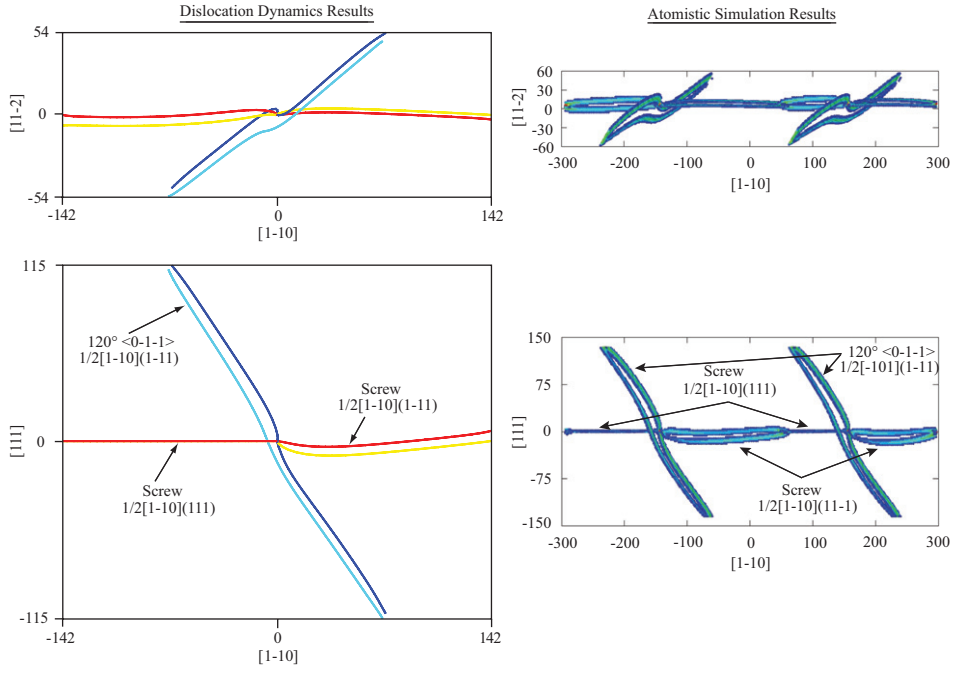

Figure 12. A comparison of the dislocation dynamics results for the partially cross-slipped core structure of a screw -120° intersection, with atomistic simulation results. [111] (x–y plane) and [11$\bar{2}$] (x–z plane) projections are shown for each case. The axes dimensions are in units of Burgers vector magnitude (2.5 Å).

conditions [8,20,21]. This is an important result since it qualitatively justifies the profuse nature of cross-slip in fcc crystals, unlike the current models for thermally-activated cross-slip that require high stress to provide a self-consistent explanation [22]. This finding should allow higher-level mesoscale models of dislocation behavior to better represent the cross-slip process without resort to *ad hoc* assumptions about obstacles.

The new cross-slip nucleation model has a variety of implications for crystal plasticity in fcc materials. For example, within the present mechanism, the frequency of cross-slip should scale with the forest dislocation density. The growth of such nuclei should depend upon the relative magnitude of local stresses on the glide plane and the cross-slip plane at the partially cross-slipped screw dislocation intersection region. Such behavior of the partially cross-slipped core under different modes of applied stress could be studied using atomistic simulations as well as dislocation dynamics simulations. Still it would be instructive to perform atomistic simulations of these screw dislocation intersection core structures in other fcc materials with different stacking fault energies (i.e. Al and Cu) to verify the results in Ni as well as determine the energy well for the partially cross-slipped intersection core configuration as a function of stacking fault energy. The stacking fault energy may also play a role in the case of extending these configurations under stress to fully accomplish the cross-slip process. The intersection mechanism of cross-slip nucleation should

also be implemented in 3D dislocation dynamics simulations as an alternative to Escaig's model in dislocation-structure evolution methods in fcc materials. Finally, it would be instructive to revisit the Bonneville and Escaig experimental results on cross-slip in fcc Cu in light of the new intersection mechanism for cross-slip nucleation [1,23].

According to Washburn [10], double intersection cross-slip, where the segment that has been pulled into the cross-slip plane soon encounters another attractive intersection that brings it back onto another primary glide plane, provides a reasonable mechanism for dislocation multiplication and the growth of slip bands at low temperatures. Naturally, such a mechanistic process must be demonstrated via modern simulation methods. Also, classical theories of strain-hardening assume that dislocation storage in Stage II of single-crystal fcc materials is a result of junction formation [24] or two-dimensional (2D) concave loop formation [25] as the gliding dislocation traverses through an array of forest dislocation obstacles on its glide plane. However, one of the major problems in classical strain-hardening models is to explain how the generation of a 3D network of stored dislocations occurs as a consequence of 2D glide [25]. We note that the intersection cross-slip nucleation mechanism for dislocation storage may provide a convenient mechanism of generating a three-dimensional network of stored dislocations from 2D glide.

The anomalous flow behavior of intermetallics (i.e. Ni_3Al) has thus far been modeled using core transformations that require thermal activation. Here again, the key issue has been that constriction energies are prohibitively high [3,4,26]. The possibility of the core transformation in the presence of interaction with other dislocations provides a novel mechanism to consider and explore in rationalizing the flow anomaly of these types of materials. However, unlike the fcc metals, it should be noted that to rationalize the increase in flow stress with temperature, a thermal component to the locking mechanism is required. It is possible that, in these materials, the dislocation interaction alone is insufficient to nucleate core transformation, but it may play a key role in lowering the activation energies since the explicit formation of a constriction is not required.

The possibility of dislocation interaction induced cross-slip nucleation raises the question of why work-hardening is found to saturate with plastic strain. The monotonic increase in dislocation density with plastic strain is well known and the attendant increase in flow stress is easily rationalized. However, the work-hardening rate itself decreases with strain. If dislocation interactions enhance cross-slip nucleation, how can a decreasing work-hardening rate with increasing dislocation density be rationalized? One possibility is that there is a critical spacing of the core-transforming nuclei beyond which there is no enhancement in cross-slip. This spacing will depend on how fast the nucleus grows, which in turn will depend on the stresses present on the two possible glide planes. Both atomistic and discrete dislocation simulations will be required to address this question properly.

5. Summary

These atomistic simulations show cross-slip nucleation can be easy during dislocation–dislocation interactions. This offers a pathway for using atomistic

simulations to identify types of interactions that result in cross-slip and use these results to rationalize in higher level mesoscale simulations such as dislocation dynamics. Summarizing the results: for a 120° ½[$\bar{1}$01] Burgers vector, ⟨0$\bar{1}\bar{1}$⟩ line direction dislocation residing on the (1$\bar{1}$1) plane intersecting a ½[1$\bar{1}$0] screw dislocation, the following observations were made using atomistic simulations of the intersection core structure using embedded atom potentials:

(1) The intersection produces five different possible core structures where the screw dislocation resides: completely on the glide (111) plane, completely on the (11$\bar{1}$) cross-slip plane in two core structures and partially on both the glide (111) and cross-slip (11$\bar{1}$) planes for two other core structures.
(2) One of the partially cross-slipped configuration for the core structure of the intersection is stable relative to the other two core structures (residing either fully on glide (111) or fully on cross-slip (11$\bar{1}$) plane) by 1.1–1.3 eV per intersection.
(3) The extended node structure for the intersections is relatively unstable with respect to the constricted structure, presumably due to the formation of significant constriction on the 120° intersecting dislocation.
(4) Dislocation dynamics simulations accounting for Shockley partials are shown to reproduce the products of dislocation intersection interacting at the atomistic level.

Acknowledgements

The authors acknowledge use of the 3D molecular dynamics code, LAAMPS, which was developed at Sandia National Laboratory by Dr. Steve Plimpton and co-workers. The authors also acknowledge use of the 'Matlab' version of 3D dislocation dynamics code, ParaDiS, which was developed at Lawrence Livermore National Laboratory by the ParaDiS team. This work was supported by the AFOSR, and by a grant of computer time from the DOD High Performance Computing Modernization Program, at the Aeronautical Systems Center/ Major Shared Resource Center. The work was performed at the U.S. Air Force Research Laboratory, Materials and Manufacturing Directorate, Wright-Patterson AFB.

References

[1] J. Bonneville and B. Escaig, Acta Metall. 27 (1979) p.1477.
[2] B. Escaig, *Proceedings of the Battelle Colloquium on Dislocation Dynamics*, A.R. Rosenfield, G.T. Hahn, A.L. Bement Jr. and R.I. Jaffee, eds., McGraw-Hill, New York, 1968, p.655.
[3] W. Puschl, Progr. Mater. Sci. 47 (2002) p.415.
[4] D. Caillard and J.L. Martin, *Thermally Activated Mechanisms in Crystal Plasticity*, Pergamon-Elsevier, Amsterdam, 2003.
[5] G. Saada, Mater. Sci. Eng. A 137 (1991) p.177.
[6] S. Rao, T.A. Parthasarathy and C. Woodward, Phil. Mag. A 79 (1999) p.1167.
[7] T. Rasmussen, K.W. Jacobsen, T. Leffers and D.B. Pedersen, Phys. Rev. B 56 (1997) p.2977.
[8] S. Rao, D.M. Dimiduk, J.A. El-Awady, T.A. Parthasarathy, M.D. Uchic and C. Woodward, to be published (2009).

[9] S. Rao, unpublished calculations (2009).
[10] J. Washburn, Appl. Phys. Lett. 7 (1965) p.183.
[11] B. Madec, B. Devincre and L.P. Kubin, Phys. Rev. Lett. 89 (2002) p.255508.
[12] S.J. Plimpton, J. Comput. Phys. 117 (1995) p.1.
[13] A.N. Stroh, Phil. Mag. 3 (1959) p.625.
[14] J.E. Angelo, N.R. Moody and M.I. Baskes, Model. Simulat. Mater. Sci. Eng. 3 (1995) p.289.
[15] V. Bulatov and W. Cai, *Computer Simulations of Dislocations*, Vol. 3, Oxford University Press, Oxford, 2006.
[16] E. Martinez, J. Marian, A. Arsenlis, M. Victoria and J.M. Perlado, J. Mech. Phys. Solid. 56 (2008) p.869.
[17] A.N. Stroh, Proc. Phys. Soc. B 67 (1954) p.427.
[18] D. Rodney, Acta Mater. 52 (2004) p.607.
[19] D. Rodney and R. Phillips, Phys. Rev. Lett. 82 (1999) p.1704.
[20] L.M. Brown, Phil. Mag. A 82 (2002) p.1691.
[21] T. Vegge and K.W. Jacobsen, J. Phys. Condens. Matter 14 (2002) p.2929.
[22] L. Kubin, T. Hoc and B. Devincre, Acta Mater. (2009), available online at http://www.sciencedirect.com.
[23] J. Bonneville, B. Escaig and J.L. Martin, Acta Metall. 36 (1988) p.1989.
[24] B. Devincre, T. Hoc and L. Kubin, Science 320 (2008) p.1745.
[25] U.F. Kocks and H. Mecking, Progr. Mater. Sci. 48 (2003) p.102.
[26] T.A. Parthasarathy and D. Dimiduk, Acta Mater. 44 (1996) p.2237.